Effect of microstrain on the magnetic properties of BiFeO3 nanoparticles

Pavana S. V. Mocherla, C. Karthik, R. Ubic, M. S. Ramachandra Rao, and C. Sudakar

Citation: Applied Physics Letters **105**, 132409 (2014); doi: 10.1063/1.4897143
View online: http://dx.doi.org/10.1063/1.4897143
View Table of Contents: http://scitation.aip.org/content/aip/journal/apl/105/13?ver=pdfcov
Published by the AIP Publishing

Effect of microstrain on the magnetic properties of $BiFeO_3$ nanoparticles

Pavana S. V. Mocherla,[1] C. Karthik,[2] R. Ubic,[2] M. S. Ramachandra Rao,[3] and C. Sudakar[1,a)]

[1]*Multifunctional Materials Laboratory, Department of Physics, Indian Institute of Technology Madras, Chennai 600036, India*

[2]*Department of Materials Science and Engineering, Boise State University, 1910 University Drive, Boise, Idaho 83725, USA*

[3]*Department of Physics and Nano Functional Materials Technology Centre, Indian Institute of Technology Madras, Chennai 600036, India*

(Received 18 June 2014; accepted 20 September 2014; published online 1 October 2014)

We report on size induced microstrain-dependent magnetic properties of $BiFeO_3$ nanoparticles. The microstrain is found to be high ($\varepsilon > 0.3\%$) for smaller crystallite sizes ($d < 30$ nm), and shows a sharp decrease as the particle size increases. The presence of pseudo-cubic symmetry is evidenced for these nanoparticles. Raman spectral studies suggest straightening of the Fe-O-Fe bond angle accompanied by a decrease in FeO_6 octahedral rotation for $d < 65$ nm. The magnetization shows a dip around 30 nm, half the size of spin cycloid length for $BiFeO_3$, due to a decrease in rhombohedral distortion with crystallite size. We also observe a similar trend in the T_N with respect to size indicating that the microstrain plays a significant role in controlling the magnetic property of $BiFeO_3$. © *2014 AIP Publishing LLC*. [http://dx.doi.org/10.1063/1.4897143]

Magnetoelectric multiferroic materials exhibit a coupling between electric, magnetic, and structural order parameters, thus, providing a new degree of freedom to tune their physical properties.[1,2] A recent surge in the research activity on these materials is due to their suitability in applications such as magnetic switches, magnetic memories, actuators, and sensors. $BiFeO_3$ (BFO) is a room-temperature magnetoelectric multiferroic material. It is a G-type antiferromagnet with $T_N \sim 643$ K and ferroelectric with $T_C \sim 1143$ K; however, the coupling between ferroelectric and magnetic order parameters, caused by alternate rotation of oxygen octahedra, is rather weak. The octahedral rotation in $BiFeO_3$ results in a slight canting of magnetic moments giving rise to a long-range spin cycloid structure with a period of ~62 nm.[3,4] The termination of spin cycloid in $BiFeO_3$ nanoparticles of size below 62 nm can give rise to a weak ferromagnetism due to the presence of uncompensated spins on the surface of the particles. Park *et al.*[5] reported the size dependent magnetic properties of $BiFeO_3$ with the lowest particle size of 14 nm. The increase in saturation magnetization (M_S) with the decrease in particle size was attributed to this suppression of spin cycloid. Similar results were reported by Mazumder *et al.*,[6] where 4 nm sized $BiFeO_3$ particles showed larger magnetization (0.41 μ_B/Fe) compared to those with larger size. Further, enhanced magnetization in $BiFeO_3$ has been reported by various groups by doping alkaline earth metal and transition metal elements at Bi and Fe sites, respectively.[7–10] In addition, studies on $BiFeO_3$ thin films showed an the increase in magnetization at low magnetic fields along with a considerable increase in polarization of the films.[11] Also, it has been shown that the magnetization in $BiFeO_3$ can be improved by adopting novel synthesis routes compared to conventional techniques.[12] Adequate research has been done to improve the magnetization; these studies also include discussions on the effect of lattice strain relaxation in $BiFeO_3$ thin films.[13,14] However, the role of microstrain in altering the magnetization of $BiFeO_3$ nanoparticles is not discussed in detail, making it an indispensable study at this juncture. Strain engineering to control physical properties of materials is an emerging area of research, in particular oxides.[15,16] In our previous study, we showed that the microstrain changes systematically with crystallite size (d in nm), which in turn controls the bandgap of the $BiFeO_3$ nanoparticles.[17]

In this report, we present the magnetic properties of these microstrain controlled $BiFeO_3$ nanoparticles. We observe a drastic reduction in the M_S around 30 nm, which is approximately half the size of spin cycloid (62 nm). We discuss how the particle size dependent microstrain and associated structural changes affect the magnetization in $BiFeO_3$ nanoparticles.

$BiFeO_3$ nanoparticles of sizes ranging from 5 to 500 nm are synthesized using a low temperature citrate sol-gel process.[17] The details of synthesis and particle size control of $BiFeO_3$ (BFO-d) are discussed in the supplementary material (also see supplementary Fig. S1).[18] Average crystallite sizes were calculated from X-ray diffraction (XRD) studies and are found to be consistent with the particle size obtained from TEM.[17] In Fig. 1, we present collated data showing the size dependent structural changes and magnetization as derived from XRD, Raman spectra, and magnetic measurements, which are subsequently discussed in the following sections. XRD and high resolution transmission electron microscopy (HRTEM) studies on the calcined samples showed structural changes in $BiFeO_3$ nanoparticles with decreasing crystallite size. More specifically, the lattice parameter "c" shows a decreasing trend from 13.892 Å for BFO-65 to 13.850 Å for BFO-22, with no significant change in "a." This decreasing trend of "c/a" ratio (Fig. 1(b)) with size is

a)Author to whom correspondence should be addressed. Electronic mail: csudakar@iitm.ac.in. Tel.: +91-44-22574895

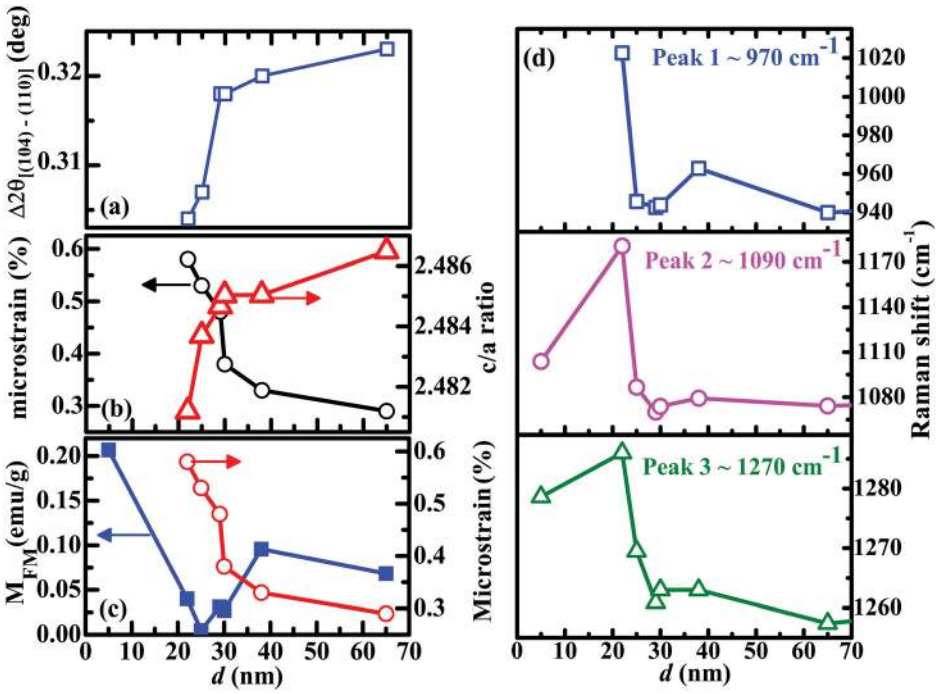

FIG. 1. (a) $\Delta 2\theta$ [(104)–(110)], (b) c/a ratio and microstrain (%) as a function of crystallite size. (c) Magnetization at 2 T after subtracting the linear part (M_{FM}) and microstrain plotted vs. the crystallite size of $BiFeO_3$ nanoparticles. (d) The two phonon mode peak positions as a function of particle size.

similar to the observation made by Selbach *et al.*,[19] where a structural change from rhombohedrally distorted (*R3c*) $BiFeO_3$ to more symmetric cubic phase ($Pm\bar{3}m$) is reported. This is also evidenced from the reduced separation of (104) and (110) peak positions [$\Delta 2\theta_{(104)-110)}$] of $BiFeO_3$ nanoparticles (Fig. 1(a) and supplementary Fig. S2).[17,18] These intense reflections are characteristic peaks of bulk $BiFeO_3$ with rhombohedrally distorted perovskite structure. An ideal cubic perovskite structure with no distortion shows only a single peak (200) around the position $2\theta^\circ = 32^\circ$. Hence, the reduction in the separation between the reflections (110) and (104) indicates a structural change in the nanoparticles. Also, the microstrain ($\varepsilon\%$) estimated from the XRD peak broadening is found to be high (>0.3%) for smaller crystallite sizes (<30 nm) and reduces with increase in size (Fig. 1(b)). This systematic increase in microstrain with decreasing $\Delta 2\theta$ and *c*/*a* ratio indicates a strain induced structural change in $BiFeO_3$ nanoparticles. Microstrain in nanoparticles can arise from the surface restructuring or due to the localized disturbances in the lattice caused by the oxygen vacancies. These structural variations are also evidenced from the HRTEM studies and are found to be highly localized (Fig. 2). Fast Fourier transform (FFT) on lattice image of BFO-22, taken at two different regions within the same crystallite, showed two different 4-fold symmetry angles, 88° and 90° (Fig. 2(c)), confirming the coexistence of rhombohedral and cubic symmetries. Filtered inverse FFT images further show the presence of compressive and tensile strains in these particles (Fig. 2(d)). FFT and inverse FFT images on BFO-38 and BFO-65 samples show that the strains in the nanoparticles reduce with increase in size (see supplementary Fig. S4).[18] Thus, microstrains reduce the rhombohedral distortion in $BiFeO_3$ leading to pseudo-cubic structure locally.

Raman spectra provide information on defects and structure at the molecular level in addition to the phase purity in nanosize $BiFeO_3$. We carried out Raman spectra on all the samples with a Horiba Jobin-Yvon (HR 800UV) micro-Raman using a 632 nm excitation line from a He-Ne laser. All these spectra were recorded at room temperature in the range 100–1500 cm^{-1} (Fig. 3). It is well known that $BiFeO_3$ exhibits a total of 13 ($4A_1 + 9E$) Raman active (also IR active) modes.[20] BFO-5, in which the crystallites are just

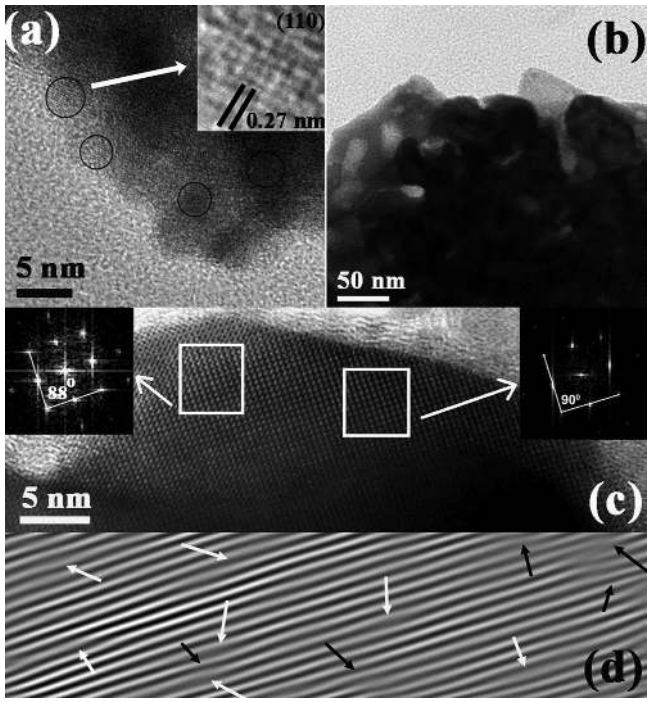

FIG. 2. (a) HRTEM image of $BiFeO_3$ precursor annealed at 350 °C showing local crystalline regions of size ~5 nm embedded in the amorphous matrix. Inset shows one such region with characteristic four-fold symmetry. (b) Bright field image of $BiFeO_3$ annealed at 375 °C (BFO-22) showing crystallites covered in porous organic residue. (c) HRTEM image of one of the crystallites of BFO-22. (Inset) Left FFT exhibits a rhombohedral distortion with 88° and the right FFT shows cubic symmetry with 90° suggesting the local structural changes in highly strained BFO-22 crystallite. (d) Filtered lattice image obtained from selectively masked FFT of the same crystallite showing compressive (black arrows) and tensile (white arrows) strains.

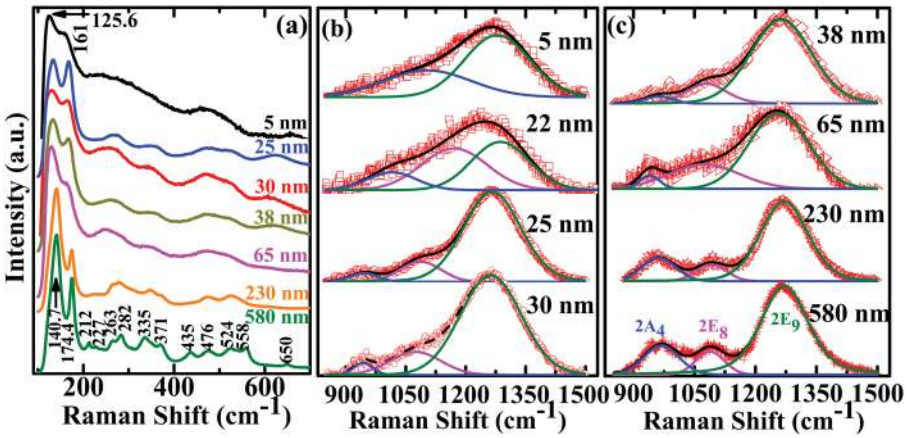

FIG. 3. (a) Representative Raman spectra of $BiFeO_3$ nanoparticles with varying crystallite sizes. Sample with large crystallite size (580 nm) shows all the modes pertaining to the rhombohedral structure of $BiFeO_3$. A_1(TO) mode at $\sim$125 cm^{-1} which is seen in nanoparticles below 65 nm disappears as the particle size increases giving rise to strong E(TO) mode at $\sim$140 cm^{-1}. (b) and (c) show the variation of two-phonon mode centered at $\sim$1260 cm^{-1}. The $2A_4$ mode reduces in intensity and $2E_8$ mode gets broadened as the size reduces.

evolving from amorphous phase (Fig. 3(a)), also has characteristic spectral features similar to bulk $BiFeO_3$ revealing the compositional homogeneity at the molecular level. Presence of even a small amount of iron oxide phase in the samples can be discerned easily due to the strong Raman scattering of Fe_2O_3 or Fe_3O_4 compounds.[21–23] Since the spectral signature in all the samples corresponds to that of $BiFeO_3$ alone and no additional modes are observed, we understand that our samples are devoid of secondary phases like Fe_2O_3, Fe_3O_4, and Bi_2O_3.[24]

Raman studies on $BiFeO_3$ have been widely reported for different morphologies like single crystals,[20,25,26] thin films,[27] polycrystalline,[28,29] and nanoparticles.[30,31] There is a large disparity in the positions, intensities, and symmetry assignments of the observed Raman modes of $BiFeO_3$ done by different groups.[20,27,28,31,32] The larger sized $BiFeO_3$ particle, i.e., BFO-580, shows two strong modes at 140 and 174 cm^{-1}. These values are close to the positions 136 and 167 cm^{-1} observed by Kothari *et al.*,[28] who assigned them to A_1 Raman modes. On the other hand, Jaiswal *et al.*,[31] assigned A_1 symmetry only to 175 cm^{-1} mode, and the other strong modes at 74, 139, and 430 cm^{-1} to E_1 symmetry.

Besides the first two modes at 140 and 174 cm^{-1} in BFO-580, the other modes are seen at 212, 227, 263, 282, 335, 371, 435, 476, 524, 558, and 650 cm^{-1} (Fig. 3(a)). All these values match very close with the data reported by Palai *et al.*[20] According to their study, the 140 cm^{-1} and 174 cm^{-1} modes correspond to the E(TO) vibrations. These prominent and well-resolved modes, however, are seen at $\sim$129 and 168 cm^{-1} in the spectra of smaller sized particles (<65 nm). These positions correspond to the A_1(TO) modes of single crystal data.[20] Also, for samples with size less than 65 nm, we only observed broad bands centered around 260, 350, and 522 cm^{-1}, all A_1(LO) modes as reported by Palai *et al.*,[20] with a broad band positioned at $\sim$470 cm^{-1} being exceptionally an E(TO) mode. In the present study, the E(TO) pair at 140 and 174 cm^{-1} is seen for $d > 65$ nm, whereas A_1(TO) pair at 129 and 168 cm^{-1} is prominent in the nanosized samples for $d < 65$ nm. It has been reported that the low frequency E(TO) (<200 cm^{-1}) modes correspond to Bi centered activity of Bi-O bonds and high frequency modes are dominated by oxygen vibrations.[30,32] A similar observation on size dependent infra-red spectra of $BiFeO_3$ has been reported by Chen *et al.*,[30] wherein the damping of E(TO) modes was attributed to the finite size effects leading to a phase transition from ferroelectric rhombohedrally distorted structure (*R3c*) to paraelectric cubic symmetry ($Pm\bar{3}m$). This phase transition in $BiFeO_3$ is highly sensitive to external perturbations like temperature, pressure, and stress.[33] It has been discerned from our XRD and TEM analyses that with reduction in particle size, the rhombohedral distortion present in $BiFeO_3$ (*R3c*) ceases and becomes more pseudo-cubic ($Pm\bar{3}m$). This local structural change, caused by microstrain, is accompanied by straightening of Fe-O-Fe bonds possibly leading to a decrease in the FeO_6 octahedral rotation.[34]

$BiFeO_3$ exhibits a characteristic broad band in the range $\sim$1000–1300 cm^{-1}, which according to Ramirez *et al.*,[27] are due to the two-phonon modes of A_1(LO) at 480 cm^{-1} and E(TO) modes at 550 and 620 cm^{-1}. In the present study, we observe similar two-phonon modes at $\sim$969, 1088, and 1271 cm^{-1} for BFO-580, which are overtones of modes at $\sim$476, 558, and 650 cm^{-1}. These high frequency E(TO) modes are due to Fe-O bonds.[20,32] We observe a systematic change in the relative intensity and peak position of these two-phonon modes (Figs. 2(b) and 2(c)). The intensity of the mode $\sim$969 cm^{-1} decreases steadily with decreasing particle size, whereas that of the mode at $\sim$1088 cm^{-1} has been found to increase. This behavior is attributed to the change in Fe-O-Fe bond angle due to the microstrain present in the nanoparticles. As the structure goes to pseudo-cubic, the Fe-O-Fe angle across the adjacent FeO_6 octahedra increases.[34] Thus, the alternative signature of A_1(TO) and E(TO) modes in nano and bulk $BiFeO_3$, respectively, at low frequency modes and systematic peak shifts (along with intensity variations) in the two-phonon mode conform to the local structural changes we inferred to via XRD and HRTEM studies.[17]

Finite size effects of $BiFeO_3$ nanoparticles were shown to exhibit intriguing magnetic properties, especially for the particle sizes less than 30 nm.[19] As we observed prominent effect of particle size and oxygen defects on optical properties,[17] we carried out magnetic measurements to see the influence of these on the M-H hysteresis and Néel transition temperature (T_N) in $BiFeO_3$ nanoparticles. The magnetic properties were measured using a Lakeshore 7410 vibrating sample magnetometer. Fig. 4(a) shows the magnetic hysteresis curves of BFO-5, BFO-22, BFO-38, and BFO-65 samples along with the as-prepared precursor (BFO-AP) powder. BFO-AP is paramagnetic as exhibited by the linear M vs. H curve. All the other samples also show a linear variation of magnetization for $H > 0.2$ T in addition to the non-linear hysteretic behavior

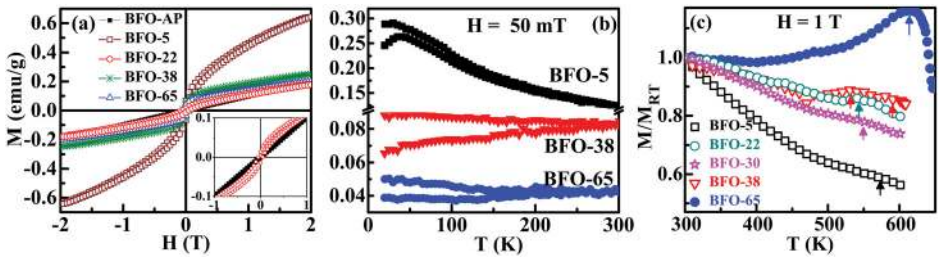

FIG. 4. (a) Room temperature M-H curves of $BiFeO_3$ nanoparticles along with BFO-AP. Inset shows the magnified portion of data corresponding to BFO-AO and BFO-22samples. (b) Low temperature ZFC-FC curves (20 K–300 K) BFO-5, BFO-38, and BFO-65 samples and (c) high temperature (300 K–700 K) M vs. T curves of BFO-5, BFO-22, BFO-30, BFO-38, and BFO-65 samples. Arrows indicate the Néel's transition in each case.

below $H \approx 0.2$ T. This indicates that the samples have a large fraction of antiferromagnetic phase in addition to a small ($\ll$1 emu/g) ferromagnetic contribution. From the M-H plots, the paramagnetic linear contribution was subtracted and the ferromagnetic magnetization (M_{FM}) value is estimated. These magnetization values are plotted with respect to particle size of $BiFeO_3$ nanoparticles in Fig. 1(c). The magnetization is highest ($M_{FM} = 0.21$ emu/g) for the BFO-5 with coercive field (Hc) of 42 mT. It should be noted that for this sample, the magnetization curve is nonlinear with continuous increase in magnetization and no saturation trend is seen up to a magnetic field of 2 T. The $BiFeO_3$ particles within the size range of 20–30 nm showed a sudden reduction in the magnetization with $M_{FM} < 0.04$ emu/g (Fig. 1(c)). For particle sizes above 30 nm, the magnetization increased first and then reduced with further increase in the particle size. Much larger particles obtained by calcining the $BiFeO_3$ precursor at 650 °C (230 nm) and 750 °C (580 nm) show no ferromagnetic magnetization (see supplementary Fig. S4(b)).[18]

BFO-5 was obtained by calcining the precursor powder at 350 °C. At this temperature, most of the organics in the sol-gel derived precursor are decomposed; however, this can lead to local reduction in the metal cations by a redox mechanism which involves the selective oxidation of hydrocarbons introducing oxygen defects in $BiFeO_3$. The formation of oxygen vacancies is mostly accompanied by a change in valence state of iron from Fe^{3+} to Fe^{2+}. However, we did not see any discernible Fe^{2+} oxidation state in BFO-5 nanoparticles from XPS studies.[17] In BFO-5, though phase formation is evident from Raman spectra, it is clear that crystallization of $BiFeO_3$ is not complete as seen from XRD and HRTEM studies. Large magnetization in BFO-5 therefore, can be attributed to these structural defects. It should be noted that such magnetization cannot be due to impurity phases such as γ-Fe_2O_3 as the magnetization will be an order of magnitude higher than what is observed in these samples.[35,36] Raman spectral studies also exclude the presence of iron oxide compounds. To assess the nature of magnetization qualitatively, we measured field-cooled (FC) and zero-field-cooled (ZFC) magnetization curves. Representative ZFC/FC magnetization data are shown in Fig. 4(b). We observe a clear peak in ZFC magnetization curve for BFO-5 with a maximum around 40 K suggesting that the local disorder induced magnetization might be the reason for impurity cluster-like magnetic properties in this sample.

For the particles of size between 20 and 30 nm, a significant reduction in magnetization is observed. This reduction is deviating largely from the continuously increasing trend in magnetization with decreasing particle size. Large surface strain results in nanoparticles with increasing surface area.[37] This surface strain can penetrate into the small particle core, leading to the randomization of spins.[38] The sharp decrease in magnetization (Fig. 1(c)) can, therefore, be accounted for by the large microstrain observed for BFO-20 to BFO-30 samples. However, a very recent report by Huang *et al.*[39] showed an anomalous deviation in magnetization around 62 nm, spin cycloid repeat distance in $BiFeO_3$. They attributed this increase in magnetization to an enhanced rotation of FeO_6 octahedra at ~62 nm. In our case, a drastic reduction in magnetization is observed at ~30 nm, half the size of spin cycloid. The sharp change in microstrain around this size seems to clearly influence the magnetization of these nanoparticles. Since the microstrain influences Fe-O-Fe bond angle and the FeO_6 octahedral tilts, the local structure is more pseudo-cubic than rhombohedrally distorted perovskite. The observations that the change in octahedral tilts affect the magnetization is consistent with the observation by Huang *et al.*[39]

For particle size >35 nm, the magnetization increases to ~0.1 emu/g and then decreases with further increase in particle size. It should be noted that for these particles (>35 nm), microstrain is reduced compared to the smaller particle sizes (20 nm–30 nm). The increased magnetization is favored by the reduced microstrain which minimizes the randomization of spins. The magnetic origin in particles with $d > 35$ nm can be understood from the following discussion. From the structural standpoint, the breaking of spin cycloid at a size lesser than 62 nm should produce uncompensated spins on the surface of the $BiFeO_3$ particles. The correlated interaction between these uncompensated spins gives rise to ferromagnetic behavior. Hence, as the particle size reduces, the magnetization is expected to increase due to the increasing ferromagnetic component over the decreasing bulk antiferromagnetic (AFM) component. We observe this trend for particle size ranging from 500 nm to 35 nm, where a steady increase in magnetization is evidenced with decreasing particle size. For BFO-65 and BFO-38, the ZFC/FC magnetization curves exhibit flat temperature dependence with a slight splitting between ZFC and FC curves. The splitting increases for BFO-38; however, no peak is observed in the ZFC/FC plot indicating the absence of nanoscale magnetic impure phases. The presence of oxygen vacancies cannot be completely ruled out in the high temperature calcined samples (BFO-38 and BFO-65). However, we believe the observed

magnetization is not due to these defects. The Fe^{2+} spins which arise due to oxygen vacancies are most likely to occupy sites adjacent to oxygen vacancies and order ferrimagnetically with neighboring Fe^{3+} spins. Fe^{2+} spins are aligned antiparallel to each other nullifying their moments in this coordination.[40] Hence, the net magnetic moment is only due to Fe^{3+} and not affected by this arrangement. Therefore, the ferromagnetic origin in $BiFeO_3$ particles above 35 nm can be attributed solely to the suppression of spin cycloid.

The particle size can also influence the AFM transition T_N in $BiFeO_3$. "M vs. T" measurements were carried out from 300 K to 800 K during the heating cycle with an applied magnetic field of 1 T. These data show a characteristic T_N in the temperature ranging from 540 K to 615 K for different particle sizes as marked by arrows in Fig. 4(c). With the increasing particle size, T_N decreases first and then increases with further increase in size, which is consistent with the magnetization trend seen in M vs. H measurements. Néel transition is very broad for BFO-22 and BFO-30 samples and occurs at a temperature much less than that of BFO-65. This indicates T_N is affected by the particle size which is in agreement with the reports by Selbach *et al.*[19] However, in our case, for BFO-5, the T_N is $\sim 580 \pm 20$ K, which is higher than that observed for BFO-22 and BFO-30 ($T_N \sim 544 \pm 20$ K). Such a change indicates that the T_N is affected not only by the particle size but also by the microstrain.

In conclusion, a strong size dependence of microstrain has been observed in $BiFeO_3$ nanoparticles of size ranging from 5 nm to 65 nm. Presence of oxygen defects and size induced surface disorder contribute to this microstrain. HRTEM images substantiate the presence of local compressive and tensile strains in the $BiFeO_3$ nanoparticles (<30 nm). Raman studies show that for $d < 65$ nm, the size of spin cycloid, A_1(TO) modes (129 and 168 cm^{-1}) are prominent in contrast to the presence of strong E(TO) modes at 140 and 174 cm^{-1} for $d > 65$ nm indicating size-selective activation of Raman modes at low frequency. In addition, peak shift accompanied with a systematic intensity reduction of two-phonon modes with size is attributed to the localized changes in Fe-O-Fe bond angle due to microstrain. Microstrain has a significant influence on the magnetic properties of $BiFeO_3$ nanoparticles, especially with in the size range 22 nm–30 nm, as inferred from the M vs. T measurements and diffuseness of Néel transition for $BiFeO_3$ nanoparticles. Our studies suggest that microstrain in nanoparticles can be used to control the magnetic properties.

The authors acknowledge the Boise State Center for Materials Characterization for TEM facility and SAIF, IIT Madras for magnetic measurements. P.S.V.M. acknowledges UGC for the senior research fellowship.

[1]G. Lawes and G. Srinivasan, J. Phys. D: Appl. Phys. **44**(24), 243001 (2011).
[2]M. Fiebig, J. Phys. D: Appl. Phys. **38**(8), R123 (2005).
[3]I. Sosnowska, T. P. Neumaier, and E. Steichele, J. Phys. C: Solid State Phys. **15**(23), 4835 (1982).
[4]H. Feng, J. Magn. Magn. Mater. **322**(13), 1765–1769 (2010).
[5]T.-J. Park, G. C. Papaefthymiou, A. J. Viescas, A. R. Moodenbaugh, and S. S. Wong, Nano Lett. **7**(3), 766–772 (2007).
[6]R. Mazumder, P. S. Devi, D. Bhattacharya, P. Choudhury, A. Sen, and M. Raja, Appl. Phys. Lett. **91**(6), 062510 (2007).
[7]B. Bhushan, D. Das, A. Priyam, N. Y. Vasanthacharya, and S. Kumar, Mater. Chem. Phys. **135**(1), 144–149 (2012).
[8]J. Liu, L. Fang, F. Zheng, S. Ju, and M. Shen, Appl. Phys. Lett. **95**(2), 022511 (2009).
[9]I. Sosnowska, W. Schäfer, W. Kockelmann, K. H. Andersen, and I. O. Troyanchuk, Appl. Phys. A **74**(Suppl. II), S1040–S1042 (2002).
[10]V. A. Khomchenko, D. A. Kiselev, E. K. Selezneva, J. M. Vieira, A. M. L. Lopes, Y. G. Pogorelov, J. P. Araujo, and A. L. Kholkin, Mater. Lett. **62**(12–13), 1927–1929 (2008).
[11]F. Bai, J. Wang, M. Wuttig, J. Li, N. Wang, A. P. Pyatakov, A. K. Zvezdin, L. E. Cross, and D. Viehland, Appl. Phys. Lett. **86**(3), 032511 (2005).
[12]K. L. Da Silva, D. Menzel, A. Feldhoff, C. Kübel, M. Bruns, A. Paesano, A. Duüvel, M. Wilkening, M. Ghafari, H. Hahn, F. J. Litterst, P. Heitjans, K. D. Becker, and V. Sěpelák, J. Phys. Chem. C **115**(15), 7209–7217 (2011).
[13]S. H. Lim, M. Murakami, W. L. Sarney, S. Q. Ren, A. Varatharajan, V. Nagarajan, S. Fujino, M. Wuttig, I. Takeuchi, and L. G. Salamanca-Riba, Adv. Funct. Mater. **17**(14), 2594–2599 (2007).
[14]J. Wang, J. B. Neaton, H. Zheng, V. Nagarajan, S. B. Ogale, B. Liu, D. Viehland, V. Vaithyanathan, D. G. Schlom, U. V. Waghmare, N. A. Spaldin, K. M. Rabe, M. Wuttig, and R. Ramesh, Science **299**(5613), 1719–1722 (2003).
[15]J. Li, Z. Shan, and E. Ma, MRS Bull. **39**(02), 108–114 (2014).
[16]D. G. Schlom, L.-Q. Chen, C. J. Fennie, V. Gopalan, D. A. Muller, X. Pan, R. Ramesh, and R. Uecker, MRS Bull. **39**(02), 118–130 (2014).
[17]P. S. V. Mocherla, C. Karthik, R. Ubic, M. S. Ramachandra Rao, and C. Sudakar, Appl. Phys. Lett. **103**(2), 022910 (2013).
[18]See supplementary material at http://dx.doi.org/10.1063/1.4897143 for more details on the preparation, TGA, XRD TEM, and magnetic measurements for $BiFeO_3$ nanoparticles.
[19]S. M. Selbach, T. Tybell, M.-A. Einarsrud, and T. Grande, Chem. Mater. **19**(26), 6478–6484 (2007).
[20]R. Palai, H. Schmid, J. F. Scott, and R. S. Katiyar, Phys. Rev. B **81**(6), 064110 (2010).
[21]C. Pascal, J. L. Pascal, F. Favier, M. L. Elidrissi Moubtassim, and C. Payen, Chem. Mater. **11**(1), 141–147 (1999).
[22]S. H. Shim and T. S. Duffy, Am. Mineral. **87**(2–3), 318–326 (2002).
[23]O. N. Shebanova and P. Lazor, J. Raman Spectrosc. **34**(11), 845–852 (2003).
[24]V. N. Denisov, A. N. Ivlev, A. S. Lipin, B. N. Mavrin, and V. G. Orlov, J. Phys.: Condens. Matter **9**(23), 4967 (1997).
[25]R. Haumont, J. Kreisel, P. Bouvier, and F. Hippert, Phys. Rev. B **73**(13), 132101 (2006).
[26]H. Fukumura, H. Harima, K. Kisoda, M. Tamada, Y. Noguchi, and M. Miyayama, J. Magn. Magn. Mater. **310**(2), e367–e369 (2007).
[27]M. O. Ramirez, M. Krishnamurthi, S. Denev, A. Kumar, S.-Y. Yang, Y.-H. Chu, E. Saiz, J. Seidel, A. P. Pyatakov, A. Bush, D. Viehland, J. Orenstein, R. Ramesh, and V. Gopalan, Appl. Phys. Lett. **92**(2), 022511 (2008).
[28]D. Kothari, V. Raghavendra Reddy, V. G. Sathe, A. Gupta, A. Banerjee, and A. M. Awasthi, J. Magn. Magn. Mater. **320**(3–4), 548–552 (2008).
[29]A. A. Porporati, K. Tsuji, M. Valant, A.-K. Axelsson, and G. Pezzotti, J. Raman Spectrosc. **41**(1), 84–87 (2010).
[30]P. Chen, X. Xu, C. Koenigsmann, A. C. Santulli, S. S. Wong, and J. L. Musfeldt, Nano Lett. **10**(11), 4526–4532 (2010).
[31]A. Jaiswal, R. Das, T. Maity, K. Vivekanand, S. Adyanthaya, and P. Poddar, J. Phys. Chem. C **114**(29), 12432–12439 (2010).
[32]P. Hermet, M. Goffinet, J. Kreisel, and P. Ghosez, Phys. Rev. B **75**(22), 220102 (2007).
[33]R. Haumont, J. Kreisel, and P. Bouvier, Phase Transitions **79**(12), 1043–1064 (2006).
[34]A. Palewicz, R. Przenioslo, I. Sosnowska, and A. W. Hewat, Acta Crystallogr., Sect. B: Struct. Sci. **63**(4), 537–544 (2007).
[35]C. Caizer, Physica B **327**(1), 27–33 (2003).
[36]H. Bea, M. Bibes, A. Barthelemy, K. Bouzehouane, E. Jacquet, A. Khodan, J.-P. Contour, S. Fusil, F. Wyczisk, A. Forget, D. Lebeugle, D. Colson, and M. Viret, Appl. Phys. Lett. **87**(7), 072508 (2005).
[37]G. Ouyang, W. G. Zhu, C. Q. Sun, Z. M. Zhu, and S. Z. Liao, Phys. Chem. Chem. Phys. **12**(7), 1543–1549 (2010).
[38]G. C. Papaefthymiou, J. Magn. Magn. Mater. **272–276**, E1227–E1229 (2004).
[39]F. Huang, Z. Wang, X. Lu, J. Zhang, K. Min, W. Lin, R. Ti, T. Xu, J. He, C. Yue, and J. Zhu, Sci. Rep. **3**, 2907 (2013).
[40]C. Ederer and N. A. Spaldin, Phys. Rev. B **71**(22), 224103 (2005).